

Hetero-metal Mn-Cu and Mn-Ni Clusters with Tridentate Schiff-base Ligands

Masayuki Nihei, Ayano Yoshida, Satoshi Koizumi, and Hiroki Oshio.*

Graduate School of Pure and Applied Sciences, University of Tsukuba, Tennodai 1-1-1,

Tsukuba 305-8571, Japan

Keywords: Schiff base ligand, heterometal cluster, multi-nuclear cluster, manganese, magnetism.

Abstract

Novel hetero-metal di-, tetra-, and octanuclear Mn-Cu clusters of $[\text{Mn}^{\text{III}}\text{Cu}^{\text{II}}(5\text{-Br-sap})_2\text{Cl}(\text{EtOH})]$ (**1**), $[\text{Mn}^{\text{III}}\text{Cu}^{\text{II}}(5\text{-Cl-sap})_2\text{Cl}(\text{MeOH})]$ (**2**), $[\text{Mn}^{\text{III}}_2\text{Cu}^{\text{II}}_2(5\text{-Br-sap})_4(\text{H}_2\text{O})_2](\text{ClO}_4)_2$ (**3**(ClO_4)₂), $[\text{Mn}^{\text{III}}\text{Cu}^{\text{II}}_3(5\text{-Br-sae})_4(\text{H}_2\text{O})_2](\text{PF}_6)_2 \cdot 2\text{Et}_2\text{O}$ (**4**(PF_6)₂·2Et₂O), $[\text{Mn}^{\text{III}}_2\text{Mn}^{\text{II}}_2\text{Cu}^{\text{II}}_4(3\text{-OMe-sap})_4(\mu_4\text{-O})_2(\mu_2\text{-OMe})_2\text{Cl}_2]\text{Cl}_2 \cdot 2\text{MeOH}$ (**5**Cl₂·2MeOH), as well as tetranuclear Mn-Ni clusters of $[\text{Mn}^{\text{III}}_2\text{Ni}^{\text{II}}_2(\text{sap})_2(\text{sal})_2(\mu_3\text{-OMe})_2(\text{OAc})_2]$ (**6**), $[\text{Mn}^{\text{III}}_2\text{Ni}^{\text{II}}_2(\text{sap})_2(\text{sal})_2(\mu_3\text{-OMe})_2(\text{NO}_3)_2(\text{MeOH})_2]$ (**7**) were prepared by simple one-pot reactions of multidentate Schiff base ligands with metal sources. All

clusters were selectively obtained by changing reaction conditions, employment of suitable co-ligands, and slightly modified ligands. We report here syntheses, structure and magnetic properties of a series of hetero-metal Mn-Cu and Mn-Ni clusters.

1. Introduction

Multi-nuclear clusters have been known to show intriguing reactivity and physical properties originating from electronic and magnetic interactions between metal ions, among which polynuclear manganese clusters have been attracted much interest from the view points of bio-inorganic and physical aspects such as mimic of active sites in photosystem II (PSII)[1-5] and single-molecule magnets (SMMs)[6]. A great deal of efforts has been made to explore rational synthetic methods for multi-nuclear manganese clusters. In this context, we have found that multidentate Schiff base ligands with alkoxo groups are useful bridging ligands to afford various multi-nuclear metal clusters, some of which were proven to be SMMs.[7-11] Hetero-metal clusters are, on the other hands, very interesting research target with respect to synergy of hetero-metal ions, which may lead to particular

properties such as high catalytic ability or high spin ground state with large magnetic anisotropy. A well-known synthetic path for hetero-metal systems contains step-by-step reactions of different metal ions with ligands such as macro-cycles.[12] In this synthesis, ligands should have multi-coordination sites, in which each coordination site possesses different affinity of metal ions. We have previously found that Schiff base tridentate ligands have potential to afford hetero-metal clusters by facile one-pot reactions, and an alkoxo-bridged Mn-Cu dinuclear complex with the Schiff base ligand was proven to be an SMM with an $S = 5/2$ spin ground state.[13] In the reactions, slight differences of consecutive stability constants between metal ions and the ligands achieved the selective formation of hetero-metal complexes. During the course of our work to obtain larger hetero-metal clusters, we found that this synthetic method with different reaction conditions, suitable co-ligands, and slight modifications of ligand structures yielded various hetero-metal clusters. We report here syntheses, structures and magnetic properties of multi-nuclear Mn-Cu and Mn-Ni clusters.

2. Experimental

2-1. Syntheses

All reagents were purchased and used without further purification. Schiff base ligands of H₂5-Br-sae, H₂3-OMe-sap, H₂5-Br-sap, and H₂sap were prepared by condensation reactions of corresponding salicylaldehyde with aminoethyl alcohol or aminopropyl alcohol.

[Mn^{III}Cu^{II}(5-Br-sap)₂Cl(EtOH)] (1): 5-Br-salicylaldehyde (201 mg, 1.0 mmol), 3-aminopropanol (75 mg, 1.0 mmol) and triethylamine (202 mg, 2.0 mmol) were dissolved in ethanol (20 ml), forming yellow solution. MnCl₂·4H₂O (198 mg, 1.0 mmol) in ethanol (10 ml) was added to the yellow solution to obtain dark brown solution, and CuCl₂·2H₂O (56 mg, 0.33 mmol) in ethanol (10 ml) was added. The reaction mixture was allowed to stand for overnight to give dark brown crystals of **1**. Anal. Calcd for C₂₂H₂₆N₂Br₂Cl₁Cu₁Mn₁O₅·C₂H₅OH·H₂O: C, 37.13; H, 4.41; N, 3.61; Cu, 8.92; Mn, 7.71. Found: C, 37.03; H, 4.22; N, 3.46; Cu, 8.33; Mn, 7.47.

[Mn^{III}Cu^{II}(5-Cl-sap)₂Cl(MeOH)] (2): Dark brown crystals of **2** were obtained in the same manner as **1** using 5-Cl-salicylaldehyde as a starting

material. Anal. Calcd for $C_{21}H_{24}N_2Cl_3Cu_1Mn_1O_5 \cdot H_2O$: C, 40.21; H, 4.17; N, 4.46; Cu, 10.43; Mn, 9.02. Found: C, 40.19; H, 3.56; N, 4.47; Cu, 10.29; Mn, 9.21.

$[Mn^{III}_2Cu^{II}_2(5-Br-sap)_4(H_2O)_2](ClO_4)_2 \cdot 3(ClO_4)_2$: 5-Br-salicylaldehyde (201 mg, 1.0 mmol), 3-aminopropanol (75 mg, 1.0 mmol) and triethylamine (202 mg, 2.0 mmol) were dissolved in acetonitrile (10 ml), forming yellow solution. $Mn(ClO_4)_2 \cdot 6H_2O$ (288 mg, 1.0 mmol) in acetonitrile (10 ml) was added to the yellow solution to give dark brown solution and $Cu(ClO_4)_2 \cdot 6H_2O$ (124 mg, 0.33 mmol) in acetonitrile (10 ml) was added. The reaction mixture was allowed to stand for 3 days to obtain dark brown crystals of $3(ClO_4)_2$. Anal. Calcd for $C_{40}H_{44}N_4Br_4Cl_2Cu_2Mn_2O_{18} \cdot CH_3CN$: C, 32.81; H, 3.08; N, 4.56; Cu, 8.92; Mn, 7.71. Found: C, 32.61; H, 2.85; N, 4.26; Cu, 7.65; Mn, 7.68.

$[Mn^{III}Cu^{II}_3(5-Br-sae)_4(H_2O)_2](PF_6)_2 \cdot 2Et_2O$ (**$4(PF_6)_2 \cdot 2Et_2O$**): 5-Br-salicylaldehyde (201 mg, 1.0 mmol), 2-aminoethanol (61 mg, 1.0 mmol) and triethylamine (202 mg, 2.0 mmol) were dissolved in methanol (20 ml), forming yellow solution. $MnCl_2 \cdot 4H_2O$ (198 mg, 1.0 mmol) in methanol (10 ml) was added to the yellow solution to give dark brown

solution and $\text{CuCl}_2 \cdot 2\text{H}_2\text{O}$ (56 mg, 0.33 mmol) in methanol (10 ml) was added.

After stirring for 30 minutes, AgPF_6 was added to the reaction mixture and

AgCl was removed by suction. After standing for over night, resulting

precipitate was filtered off and dissolved in acetonitrile. The slow diffusion

of diethylether to the acetonitrile solution gave green crystals of $\mathbf{4}(\text{PF}_6) \cdot 2\text{Et}_2\text{O}$.

Anal. Calcd for $\text{C}_{36}\text{H}_{36}\text{N}_4\text{Br}_4\text{Cu}_3\text{F}_6\text{Mn}_1\text{O}_{10}\text{P}_1$: C, 31.00; H, 2.60; N, 4.02; Cu,

13.67; Mn, 3.94. Found: C, 31.35; H, 2.55; N, 3.95; Cu, 13.99; Mn, 3.73.

$[\text{Mn}^{\text{III}}_2\text{Mn}^{\text{II}}_2\text{Cu}^{\text{II}}_4(\mathbf{3}\text{-OMe-sap})_4(\mu_4\text{-O})_2(\mu_2\text{-OMe})_2\text{Cl}_2]\text{Cl}_2 \cdot 2\text{MeOH}$

($\mathbf{5Cl}_2 \cdot 2\text{MeOH}$): *o*-vaniline (152 mg, 1.0 mmol), 3-amino-1-propanol (75 mg,

1.0 mmol) and triethylamine (202 mg, 2.0 mmol) were dissolved in

methanol (20 ml), forming yellow solution. $\text{MnCl}_2 \cdot 4\text{H}_2\text{O}$ (198 mg, 1.0

mmol) in methanol (10 ml) was added to the yellow solution to give dark

brown solution, and $\text{CuCl}_2 \cdot 2\text{H}_2\text{O}$ (114 mg, 0.67 mmol) in methanol (10 ml)

was added. The reaction mixture was allowed to stand for a week to obtain

dark green crystals of $\mathbf{5Cl}_2 \cdot 2\text{MeOH}$. Anal. Calcd for

$\text{C}_{46}\text{H}_{58}\text{N}_4\text{Cl}_4\text{Cu}_4\text{Mn}_4\text{O}_{16} \cdot 2\text{H}_2\text{O}$: C, 35.08; H, 3.97; N, 3.56; Cu, 16.14; Mn,

13.95. Found: C, 35.20; H, 4.15; N, 3.29; Cu, 16.18; Mn, 13.95.

$[\text{Mn}^{\text{III}}_2\text{Ni}^{\text{II}}_2(\text{sap})_2(\text{sal})_2(\mu_3\text{-OMe})_2(\text{OAc})_2]$ (6**):** Salicylaldehyde (= Hsal, 122

mg, 1.0 mmol), 3-amino-1-propanol (75 mg, 1.0 mmol) and triethylamine (202 mg, 2.0 mmol) were dissolved in methanol (20 ml), forming yellow solution. $\text{Mn}(\text{CH}_3\text{COO})_2 \cdot 4\text{H}_2\text{O}$ (246 mg, 1.0 mmol) in methanol (10 ml) was added to the yellow solution to obtain dark brown solution. To the dark brown solution, green mixture of Hsal (122 mg, 1.0 mmol), triethylamine (202 mg, 2.0 mmol), and $\text{Ni}(\text{CH}_3\text{COO})_2 \cdot 4\text{H}_2\text{O}$ (248 mg, 1.0 mmol) in methanol (30 ml) was added. The reaction mixture was allowed to stand for one night to give dark green crystals of **6**. Anal. Calcd for $\text{C}_{40}\text{H}_{44}\text{N}_2\text{Mn}_2\text{Ni}_2\text{O}_{14} \cdot \text{H}_2\text{O}$: C, 47.00; H, 4.53; N, 2.74; Mn, 10.75; Ni, 11.48. Found: C, 47.17; H, 4.67; N, 2.67; Mn, 10.69; Ni, 11.88.

[Mn^{III}₂Ni^{II}₂(sap)₂(sal)₂(μ ₃-OMe)₂(NO₃)₂(MeOH)₂] (7): Dark green crystals of **7** were obtained in the same manner as **6** using $\text{Mn}(\text{NO}_3)_2 \cdot 6\text{H}_2\text{O}$ and $\text{Ni}(\text{NO}_3)_2 \cdot 6\text{H}_2\text{O}$ as metal sources. Anal. Calcd for $\text{C}_{38}\text{H}_{46}\text{N}_4\text{Mn}_2\text{Ni}_2\text{O}_{19}$: C, 41.87; H, 4.49; N, 5.14; Mn, 10.06; Ni, 10.75. Found: C, 41.96; H, 4.25; N, 5.05; Mn, 9.66; Ni, 10.78.

2-2. X-ray crystallography

All crystals were mounted on a glass capillary, and data were collected at -70 C° (Bruker SMART APEX diffractometer coupled with a CCD area detector with graphite monochromated Mo-K α ($\lambda = 0.71073$ Å) radiation), respectively. Structures were solved by direct methods and expanded by using Fourier techniques using SHELXTL program. Crystal data for the complexes were summarized in Table 1. Empirical absorption corrections by SADABS (G. M. Sheldrick, 1994) were carried out. In the structure analyses, non-hydrogen atoms were refined with anisotropic thermal parameters. Hydrogen atoms were included in calculated positions and refined with isotropic thermal parameters riding on those of the parent atoms. Crystallographic data reported in this paper have been deposited with Cambridge Crystallographic Data Centre as supplementary publication no. CCDC 617406, 617405, 617409, 617410, 617404, 617407, and 617408 for **1**, **2**, **3**(ClO₄)₂, **4**(PF₆)·2Et₂O, **5**Cl₂·2MeOH, **6**, and **7**, respectively. These data can be obtained free of charge via www.ccdc.cam.ac.uk/conts/retrieving.html (or from the Cambridge Crystallographic Data Centre, 12, Union Road, Cambridge CB2 1EZ, UK; fax: (+44) 1223-336-033; or deposit @ccdc.cam.ac.uk).

2-2. Physical measurements

DC magnetic susceptibility data were collected by using a Quantum Design MPMS-XL SQUID magnetometer at temperatures ranging from 1.8 to 300 K.

3. Results and Discussion

3-1. Syntheses of Mn-Cu and Mn-Ni hetero-metal clusters

The Mn-Cu and Mn-Ni hetero-metal clusters, **1-7**, were synthesized by simple reactions of multidentate schiff base ligands (H₂5-Br-sae, H₂3-OMe-sap, H₂5-Br-sap, and H₂sap) (Scheme 1), with metal sources and suitable co-ligands (Scheme 2). All reactions possessed good selectivity for the target compounds, and the selectivity can be achieved by optimization of reaction conditions. The dinuclear complex of **1** and **2** were synthesized by the reaction of tridentate Schiff base ligand (5-Br-sap²⁻) and metal chlorides with a reaction ratio of 3:3:1. The similar reaction in acetonitrile using

metal perchlorate gave a tetranuclear complex of $\mathbf{3}(\text{ClO}_4)_2$. The tetranuclear complex of $\mathbf{4}(\text{PF}_6)\cdot 2\text{Et}_2\text{O}$ was obtained by using metal chloride and 5-Br-sae²⁻ followed by removing chloride ions with AgPF₆. On the other hand, octanuclear complex of $\mathbf{5}\text{Cl}_2\cdot 2\text{MeOH}$ was synthesized by employing a quadridentate Schiff base ligand of 3-OMe-sap²⁻. Mn^{III}₂Ni^{II}₂ tetranuclear clusters of **6** and **7** were obtained by the reactions of tridentate Schiff base ligand (sap²⁻), bidentate co-ligand (sal¹⁻), and metal sources, where **6** and **7** were obtained as acetate and nitrate salts.

3-2. Descriptions of Crystal structures

3-2-1. $[\text{Mn}^{\text{III}}\text{Cu}^{\text{II}}(5\text{-Br-sap})_2\text{Cl}(\text{EtOH})]$ (**1**) and $[\text{Mn}^{\text{III}}\text{Cu}^{\text{II}}(5\text{-Cl-sap})_2\text{Cl}(\text{MeOH})]$ (**2**)

An ORTEP diagram of a Mn-Cu dinuclear complex of **1** is shown in Figure 1. **1** crystallizes in monoclinic space group $P2_1/c$ with the molecule lying on the crystallographic centre of inversion. The Crystal structure of **1** is isostructural with the previously reported dinuclear complex of $[\text{Mn}^{\text{III}}\text{Cu}^{\text{II}}(5\text{-Br-sap})_2\text{Cl}(\text{MeOH})]$ [13], and **1** has a dinuclear structure composed of a Mn^{III} and Cu^{II} core doubly bridged by two alkoxo groups. The dc magnetic susceptibility data and bond valence sum (BVS)

considerations (3.05 and 2.02 for Mn^{III} and Cu^{II} ions, respectively) support that **1** is not a 1:1 mixture but a mixed metal system. The dinuclear unit has a crystallographic inversion, and the Mn^{III} and Cu^{II} ion sites are, therefore, positionally disordered. The coordination geometry about Mn^{III} and Cu^{II} ions are presumed to be octahedral and square planer geometry, respectively. Equatorial coordination sites of the Mn^{III} ion are occupied by three oxygen atoms and one nitrogen atom from the tridentate Schiff base ligand, and the axial sites of Mn^{III} ion are occupied by an oxygen atom of coordinating ethanol molecule and a chloride ion. Coordination bond lengths in the equatorial plane are in the range of 1.871(6) – 1.959(7) Å, while the axial coordination bonds showed significant elongation (2.477(11) and 2.694(5) Å) which is due to the Jahn-Teller distortion. The coordination bond lengths for Cu^{II} ions are the same as those for the corresponding coordination bonds of Mn^{III} ion due to the crystallographic inversion centre. The Cu^{II} and Mn^{III} ions are bridged by alkoxo groups with bridging angles of 102.0(2)°. The crystallographic data and the molecular structure of **2** were similar to those of **1** except for the coordinating solvent molecule and substituent group on the ligand. The coordination bond lengths for the equatorial coordination sites

of Mn^{III} and Cu^{II} ions are 1.871(6) – 1.959(7) Å, and the Jahn-Teller axis of Mn^{III} ion involves an oxygen atom of methanol and a chloride ion with inter-atomic distances of 2.573(7) and 2.662(3) Å, respectively. BVS calculations gave values of 3.00 and 1.99 for Mn^{III} and Cu^{II} ions, respectively. The bridging angle between Mn^{III} and Cu^{II} ions (Mn1-O2-Cu1) are 101.84(15)°.

3-2-2. $[Mn^{III}_2Cu^{II}_2(5-Br-sap)_4(H_2O)_2](ClO_4)_2 \cdot 3(ClO_4)_2$

The tetranuclear complex of $3(ClO_4)_2$ crystallizes in triclinic space group $P\bar{1}$ and crystallographic inversion centre exists in the middle of the complex cation. The tetranuclear core consists of an incomplete face-sharing double cube composed of two Mn^{III} and two Cu^{II} ions (Figure 2). Assignments of metal ions were confirmed by the BVS calculations (3.22 and 2.09 for Mn^{III} and Cu^{II} ions, respectively) and the short coordination bond lengths for Mn^{III} ions. The Mn^{III} and Ni^{II} ions are doubly bridged to form a dinuclear unit by two oxygen atoms (O2 and O4), and the symmetrically related dinuclear cores are linked by two phenoxo (O1 and O1[#]) and two alkoxo groups (O4 and O4[#]) in μ_2 and μ_3 fashions, respectively. The Mn^{III}

ions have N_1O_5 chromophore in which equatorial sites and one of the axial sites are occupied by four oxygen atoms and one nitrogen atom from the Schiff base ligands and remaining axial sites are coordinated by a water molecule, leading to the distorted octahedral coordination geometry. The coordination bond lengths about Mn^{III} ions are in the range of 1.851(4) – 2.008(5) Å for the equatorial sites (Mn1-N2, O2, O3, O4), and 2.312(5) and 2.329(4) Å for the axial sites (Mn1-O5, Mn1-O1[#]). The coordination geometry of Cu^{II} ions is square pyramidal, and equatorial positions are occupied by three oxygen atoms (O1, O2, O4) and one nitrogen atom (N1) with coordination bond lengths of 1.896(4) – 2.004(4) Å. The apical position of the Cu^{II} ions is weakly coordinated by oxygen atom (O4[#]) of μ_3 -alkoxo group and the bond length of Cu1-O4[#] is 2.585(4) Å. The bridging angles between Cu^{II} and Mn^{III} ions are 96.17(16) – 105.33(17)°, while Cu1-O4-Cu1[#] is 96.94(16)°.

3-2-3. $[Mn^{III}Cu^{II}_3(5-Br-sae)_4(H_2O)_2](PF_6)\cdot 2Et_2O$ ($4(PF_6)\cdot 2Et_2O$)

The ORTEP drawing of **4** is shown in Figure 4. The crystal of $4(PF_6)\cdot 2Et_2O$ has monoclinic space group $P2/c$ and the unit cell contains two

complex cations, two counter anions, and four diethylether molecules. The complex cation is composed of a tetranuclear cubic core, in which four metal ions are bridged by four μ_3 -alkoxo groups from the Schiff base ligands. The cubic core contains two crystallographically independent metal ions with square pyramidal or distorted octahedral coordination geometries, and the two sets of metal ions are related by the crystallographic two fold axis passing through the centre of the complex cation. The valence sum considerations, elemental analysis, and dc magnetic susceptibilities measurement suggested that the complex cation is constructed by three Cu^{II} ions and one Mn^{III} ion. Consequently, the five-coordinated metal ions are assigned to Cu^{II} ions, while symmetrically related two six-coordinated metal ions can be considered to be positional disordered Mn^{III} and Cu^{II} ions, respectively. The equatorial coordination bond lengths of the square pyramidal Cu^{II} coordination sites are in the range of 1.898(5) – 1.953(5) Å, and the apical position is coordinated by an alkoxo group of the Schiff base ligand with coordination bond length of 2.511(5) Å. The positionally disordered Mn^{III} and Cu^{II} ions have distorted octahedral geometry with elongated axis along O4-Mn1-O5, and the coordination bond lengths with

axial atoms are 2.319(5) and 2.534 Å for Mn1-O5 and Mn1-O4, respectively.

Bridging angles of metal ions with alkoxo groups are in the range of 89.93(16) – 109.7(2)°.

3-2-4. $[Mn^{III}_2Mn^{II}_2Cu^{II}_4(3-OMe-sap)_4(\mu_4-O)_2(\mu_2-OMe)_2Cl_2]Cl_2 \cdot 2MeOH$ (**5** Cl_2
 $\cdot 2MeOH$)

5 $Cl_2 \cdot 2MeOH$ crystallizes in monoclinic space group $P2_1/n$ and complex cation situated on the crystallographic inversion centre. **5** has hexanuclear $Mn^{III}_2Cu^{II}_4$ core bridged by μ_4 -oxo and μ_2 -alkoxo groups, and peripheral Mn^{II} ions are attached to the Cu^{II} and Mn^{III} ions in the core by μ_2 -phenoxo- and μ_2 -methoxo-bridges, respectively. In **5**, Schiff bases act as quadridentate ligands to construct octanuclear core. The metal assignment and their oxidation states were confirmed by considering coordination bond lengths, existence of Jahn-Teller elongation, and BVS calculations (3.11, 2.06, 1.82 and 1.98 for Mn1, Mn2, Cu1 and Cu2 ions, respectively). Mn^{III} ions have a five-coordinated square pyramidal coordination geometry. The equatorial coordination sites of Mn^{III} ions are occupied by four oxygen atoms (O2, O5, O7, and O8) from two Schiff base ligands, one μ_4 -oxo and μ_2 -alkoxo groups, respectively, and O7[#] ion coordinates from the apical

position. The coordination geometries of four-coordinated Cu^{II} ions are square planer with N₁O₄ chromophore and coordination bond lengths are in the range of 1.932(3) – 2.036(2) Å and 1.911(2) – 1.959(2) Å for Cu1 and Cu2 ions, respectively. Mn^{II} ions have octahedral coordination geometry, where two Schiff base ligands coordinate to the Mn^{II} ions with phenoxy and methoxy groups acting as bidentate ligands. The remaining coordination sites are occupied by μ_2 -alkoxo and chloride ions. The coordination bond lengths of Mn^{II} ions are in the range of 2.119(3) – 2.4335(12) Å, which are apparently longer than those of Mn^{III} ions.

3-2-5. $[Mn^{III}_2Ni^{II}_2(sap)_2(sal)_2(\mu_3-OMe)_2(OAc)_2]$ (**6**) and $[Mn^{III}_2Ni^{II}_2(sap)_2(sal)_2(\mu_3-OMe)_2(NO_3)_2(MeOH)_2]$ (**7**)

The ORTEP diagrams of tetranuclear complexes **6** and **7** are shown in Figure 6 and 7. Both complexes crystallized in triclinic space group $P\bar{1}$. The complex **6** has an incomplete face-sharing double cubane core composed of two Mn^{III} and two Ni^{II} ions. The metal ions were assigned by BVS calculations and observations of Jahn-Teller elongations for the Mn^{III} ions. BVS calculations gave the values of 3.18 and 2.12 for Mn^{III} and Ni^{II} ions, respectively. The Mn^{III} ions are coordinated by tridentate Schiff base

ligands forming mononuclear units, while Ni^{II} ion constructs mononuclear unit with bidentate co-ligands (sal¹⁻). These mononuclear units are linked to form a planer Mn^{III}-Ni^{II} dinuclear unit by μ_2 -alkoxo and μ_3 -methoxo groups, where additional acetate ion bridged the Mn^{III} and Ni^{II} ions from the axial direction supporting dinuclear core. The crystallographically related two dinuclear units are bridged by μ_2 -phenoxo and μ_3 -methoxo groups to form the tetranuclear core. The equatorial sites of six-coordinated Mn^{III} ions are occupied by N1, O1, O2, O7 atoms with bond lengths of 1.865(2) – 2.021(3) Å, and the axial coordination bond lengths are 2.340(2) Å and 2.198(2) Å, which are significantly elongated due to Jahn-Teller distortions. The Ni^{II} ions with six-coordinated octahedral geometry have coordination bond lengths of 2.027(2) – 2.094(2) Å, which are longer than those of Mn^{III} ions. **7** has a similar structural feature as **6** except for the bridging structure between Mn^{III} and Ni^{II} ions. In the case of **6**, Mn^{III} and Ni^{II} ions in the dinuclear unit were bridged by μ_2 -alkoxo, μ_3 -methoxo, and μ_2 -acetato groups, while in **7** bridging μ_2 -acetato groups were replaced with methanol molecules and nitrate ions. It is noted that those different bridging structures lead to the significant difference in the magnetic interactions between Mn^{III} and Ni^{II}

ions. The equatorial coordination bond lengths of Mn^{III} ions are in the range of 1.855(4) – 2.000(4) Å, and the axial coordination bond lengths are 2.251(3) Å and 2.283(4) Å. The Ni^{II} ions have an O₆ chromophore with bond lengths of 1.998(3) – 2.109(4) Å. BVS calculations for Mn^{III} and Ni^{II} ions yielded the values of 3.19 and 2.05, which support the assignment of metal ions. The bridging angles between Ni^{II} and Mn^{III} ions for **6** and **7** are in the range of 94.19(8) – 103.61(8)° and 94.54(13) – 103.45(15)°, while the crystallographically related two Ni^{II} ions are bridged with the angles of 98.19(8)° and 97.35(14)° for **6** and **7** respectively.

3-3. Magnetic properties of the complexes 1-7

3-3-1. Magnetic properties of 1 and 2.

The dc magnetic susceptibility measurements for **1** and **2** were performed in the temperature range of 1.8 – 300 K (Figure 8). The $\chi_m T$ - T curves for **1** and **2** were very similar to that for the previously reported dinuclear complex of [Mn^{III}Cu^{II}(5-Br-sap)₂Cl(MeOH)] [13], which was proven to be an SMM with $S = 5/2$ and $D = -1.86 \text{ cm}^{-1}$. The $\chi_m T$ values at 300 K are 3.91 emu mol⁻¹ K and 3.85 emu mol⁻¹ K for **1** and **2**, respectively,

which is larger than the value ($3.375 \text{ emu mol}^{-1} \text{ K}$ with $g = 2$) expected for the uncorrelated Mn^{III} and Cu^{II} ions. The $\chi_{\text{m}}T$ values gradually increased as decreasing the temperature, reaching the plateau values of $4.23 \text{ emu mol}^{-1} \text{ K}$ and $4.03 \text{ emu mol}^{-1} \text{ K}$ for **1** (100 K) and **2** (150 K), respectively. The temperature dependences of $\chi_{\text{m}}T$ values suggested the occurrence of ferromagnetic interactions between Mn^{III} and Cu^{II} ions to give $S = 5/2$ spin ground states in **1** and **2**. The smaller $\chi_{\text{m}}T$ values in the plateau compared with the theoretical value ($4.20 \text{ emu mol}^{-1} \text{ K}$) for the $S = 5/2$ state is due to smaller g value of Mn^{III} ions than 2.0. The sudden decrease of $\chi_{\text{m}}T$ values at lower temperature region is due to intermolecular antiferromagnetic interactions and/or zero-field splitting. The magnetic susceptibility data were analyzed using spin Hamiltonian of $H = -2J_{\text{MnCu}}S_{\text{Mn}}\cdot S_{\text{Cu}}$. The least squares calculations using the data above 24 K (**1**) and 50 K (**2**) gave the best fit parameters of $J_{\text{MnCu}} = +64 \text{ cm}^{-1}$, $g_{\text{Mn}} = 1.93$, $g_{\text{Cu}} = 2.10$ for **1**, and $J_{\text{MnCu}} = +85 \text{ cm}^{-1}$, $g_{\text{Mn}} = 1.90$, $g_{\text{Cu}} = 2.08$ $\theta = -1.96 \text{ cm}^{-1}$ for **2**, where θ is intermolecular magnetic interaction. The preliminary ac magnetic susceptibility measurements for **1** and **2** showed the frequency dependent out-of-phase ac susceptibilities (Figure S1 and S2), suggesting both

complexes being SMMs.

3-3-2. Magnetic properties of 3(ClO₄)₂, 4(PF₆)·2Et₂O, and 5Cl₂·2MeOH.

The dc magnetic susceptibility measurements were carried out in the temperature range of 1.8 – 300 K and the results were depicted in Figure 9. In **3**(ClO₄)₂, the $\chi_m T$ value at 300 K is 6.80 emu mol⁻¹ K, which is a good agreement with the spin only value for magnetically isolated two Mn^{III} and two Cu^{II} ions (6.75 emu mol⁻¹ K, $g = 2$). Upon decreasing the temperature, the $\chi_m T$ value showed gradual increase down to 150 K, followed by the decrease at lower temperature, and this suggested that the ferromagnetic interactions are operative in high temperature region, followed by antiferromagnetic interactions leading to $S = 0$ spin ground state. Analyses of the susceptibility data for **3**(ClO₄)₂ were carried out by using simple butterfly model, however, curve fitting was inferior, which might be due to the simplified model, and further analysis of the magnetic data has not been done yet. In the $\chi_m T$ versus T plot for **4**(PF₆)·2Et₂O, $\chi_m T$ values shows steady decrease upon temperature was lowered, which suggests overall antiferromagnetic couplings among metal ions. The $\chi_m T$ value at 300 K is

3.38 emu mol⁻¹ K, which is smaller than the curie constant (4.13 emu mol⁻¹ K) for uncorrelated one Mn^{III} and three Cu^{II} ions. The $\chi_m T$ value reached the minimum value of 0.5 emu mol⁻¹ K at 1.8 K. The data was analyzed by using spin Hamiltonian of $H = -2J_{CuCu}(S_{Cu1} \cdot S_{Cu2} + S_{Cu2} \cdot S_{Cu3} + S_{Cu1} \cdot S_{Cu3}) - 2J_{CuMn} S_{Mn1} \cdot (S_{Cu1} + S_{Cu2} + S_{Cu3})$. The least squares calculation gave the best fit parameters of $J_{CuCu} = -12.4$ cm⁻¹, $J_{MnCu} = -18.0$ cm⁻¹, $g_{Mn} = 1.98$, and $g_{Cu} = 2.19$, with a spin ground state of $S = 1/2$. The $\chi_m T$ value at 300 K for **5**Cl₂·2MeOH is 12.38 emu mol⁻¹ K and showed constant decrease as temperature was lowered, reaching the value of 2.35 emu mol⁻¹ K at 1.8 K. The theoretical value expected for magnetically isolated four Cu^{II} and two Mn^{III} and Mn^{II} ions is 16.25 emu mol⁻¹ K and the smaller value might be due to relatively strong antiferromagnetic interactions. The $\chi_m T-T$ plot for **5**Cl₂·2MeOH indicated that overall antiferromagnetic interactions are dominant in whole temperature range and further analysis of magnetic data has not been carried out due to complicated magnetic interactions among the metal ions.

3-3-2. Magnetic properties of $[Mn^{III}_2Ni^{II}_2(sap)_2(sal)_2(\mu_3-OMe)_2(OAc)_2]$ (**6**)

and $[Mn^{III}_2Ni^{II}_2(sap)_2(sal)_2(\mu_3-OMe)_2(NO_3)_2(MeOH)_2]$ (**7**)

DC magnetic susceptibility measurements were performed on **6** and **7** in the temperature range of 1.8 - 300 K. $\chi_m T$ versus temperature plots for complex **6** and **7** are shown in Figure 10. In **6**, the $\chi_m T$ value at 300 K is 8.07 emu mol⁻¹ K, which is close to the value (8.00 emu mol⁻¹ K, $g = 2$) expected for the isolated two Mn^{III} and two Ni^{II} ions. Upon cooling the temperature, the $\chi_m T$ value gradually decreased and reached to 1.97 emu mol⁻¹ K at 1.8 K, and this suggested the occurrence of antiferromagnetic interactions among metal centers. The temperature dependence of magnetic data above 20 K was analyzed by using simplified symmetrical butterfly model with spin Hamiltonian of $H = -2J_{MnNi}(S_T^2 - S_A^2 - S_B^2) - 2J_{NiNi}(S_A^2 - S_{Cu1}^2 - S_{Cu1\#}^2)$, where $S_A = S_{Ni1} + S_{Ni1\#}$, $S_B = S_{Mn1} + S_{Mn1\#}$, $S_T = S_A + S_B$. The least squares calculation gave the fit parameters of $J_{MnNi} = -1.80$ cm⁻¹, $J_{NiNi} = -3.41$ cm⁻¹, where g_{Ni} and g_{Mn} are fixed to be 2.2 and 1.9, and the spin ground state can be considered to be an $S = 2$. The $\chi_m T$ value at 1.8 K was smaller than the Curie constant (3.00 emu mol⁻¹ K, $g = 2$) for an $S = 2$ state, which is due to zero-field splitting and/or intermolecular antiferromagnetic interactions. In complex **7**, the $\chi_m T$ value

is 8.93 emu mol⁻¹ K at 300 K is slightly larger than the spin only value of 8.00 emu mol⁻¹ K expected for a complex consisting of two Mn^{III} and two Ni^{II} noninteracting ions. As lowering the temperature, $\chi_m T$ values gradually increased, reaching a maximum value of 17.65 emu mol⁻¹ K at 5.00 K, followed by decrease down to 14.83 emu mol⁻¹ K at 1.8 K. Based on temperature dependent susceptibility data ferromagnetic interactions were operative between the Mn^{III} and Ni^{II} ions, which is contrast of **6**. The magnetic data for **7** was fitted by using the data above 20 K and the best fit parameters of $J_{\text{MnNi}} = +3.62 \text{ cm}^{-1}$, $J_{\text{NiNi}} = -7.81 \text{ cm}^{-1}$, $g_{\text{Ni}} = 2.2$ (fixed), and $g_{\text{Mn}} = 1.9$ (fixed) were obtained. The spin ground state was considered to be $S = 5$. The difference in the magnetic properties between **6** and **7** is originating from the bridging structures of the Mn^{III} and Ni^{II} ions. In **6**, the magnetic paths between Mn^{III} and Ni^{II} ions are through μ_2 -alkoxo, μ_3 -methoxo and μ_2 -acetato bridges, among which antiferromagnetic pathways through acetate bridges might be predominant, leading to the lower spin ground state of $S = 2$. On the other hands, complex **7** has high spin ground state originating from ferromagnetic interactions through μ_2 -alkoxo, μ_3 -methoxo groups, which might be due to the accidental orthogonality of the

magnetic orbitals.

Conclusion

A versatile synthetic method for multi-nuclear hetero-metal clusters has been developed, and a series of Mn-Cu clusters with the core structures of $[\text{Mn}^{\text{III}}\text{Cu}^{\text{II}}]$, $[\text{Mn}^{\text{III}}_2\text{Cu}^{\text{II}}_2]$, $[\text{Mn}^{\text{III}}\text{Cu}^{\text{II}}_3]$, and $[\text{Mn}^{\text{III}}_2\text{Mn}^{\text{II}}_2\text{Cu}^{\text{II}}_4]$, as well as Mn-Ni clusters with $[\text{Mn}^{\text{III}}_2\text{Ni}^{\text{II}}_2]$ cores were synthesized. This strategy might be applicable to prepare various 3d-3d and 3d-4f hetero-metal clusters by changing reaction conditions and slight modifications of bridging ligands. Further studies to obtain larger clusters are in progress.

Acknowledgement

This work was partially supported by a Grant-in-aid for Scientific Researches from the Ministry of Education, Culture, Sports, Science and Technology, Japan, and by the COE and TARA projects of University of Tsukuaba.

References

- [1] U. Bossek, T. Weyhermüller, K. Weighardt, B. Nuber, J. Weiss, J. Am.

- Chem. Soc. 112 (1990) 6387.
- [2] C. F. Yocum, V. L. Pecoraro, *Curr. Opin. Chem. Biol.* 3 (1999) 182.
- [3] W. Ruettinger, M. Yagi, K. Wolf, S. Bernasek, G. C. Dismukes, *J. Am. Chem. Soc.* 122 (2000) 10353.
- [4] S. Mukhopadhyay, R. J. Staples, W. H. Armstrong, *Chem. Commun.* (2002) 664.
- [5] S. Bhaduri, M. Pink, G. Christou, *Chem. Commun.* (2002) 2352.
- [6] G. Christou, D. Gatteschi, D. N. Hendrickson, R. Sessoli, *MRS Bulletin* 25 (2000) 66.
- [7] H. Oshio, N. Hoshino, T. Ito, *J. Am. Chem. Soc.* 122 (2000) 12602.
- [8] H. Oshio, N. Hoshino, T. Ito, M. Nakano, *J. Am. Chem. Soc.* 126 (2004) 8805.
- [9] S. Koizumi, M. Nihei, M. Nakano, H. Oshio, *Inorg. Chem.* 44 (2005) 1208.
- [10] H. Oshio, M. Nihei, S. Koizumi, T. Shiga, H. Nojiri, M. Nakano, N. Shirakawa, M. Akatsu, *J. Am. Chem. Soc.* 127 (2005) 4568.
- [11] H. Oshio, M. Nakano, *Chem. Eur. J.* 11 (2005) 5178.
- [12] H. Ōkawa, H. Frutachi, D. E. Fenton, *Coord. Chem. Rev.* 174 (1998)

51.

- [13] H. Oshio, M. Nihei, A. Yoshida, H. Nojiri, M. Nakano, A. Yamaguchi,
Y. Karaki, H. Ishimoto, *Chem. Eur. J.* 11 (2004) 843.

Table 1 Crystallographic Data for Complexes 1-7

	1	2	3(ClO ₄) ₂	4(PF ₆) ₂ Et ₂ O	5Cl ₂ ·2MeOH	6	7
Formula	C ₂₂ H ₂₅ Br ₃ ClCuMnN ₂ O ₅	C ₂₁ H ₂₃ Cl ₃ CuMnN ₂ O ₅	C ₄₀ H ₄₄ Br ₄ Cl ₂ Cu ₂ Mn ₂ N ₂ O ₁₈	C ₄₄ H ₅₆ Br ₄ Cu ₃ F ₆ MnN ₄ O ₁₂ P	C ₄₈ H ₆₄ Cl ₄ Cu ₄ Mn ₄ N ₄ O ₁₆	C ₄₀ H ₄₄ Mn ₂ N ₂ Ni ₂ O ₁₄	C ₃₈ H ₄₄ Mn ₂ N ₄ Ni ₂ O ₂₀
Formula weight / g mol ⁻¹	711.20	608.27	1468.28	1543.11	1568.80	1004.06	1104.05
Temp / K	200	200	200	200	200	200	200
Crystal system	Monoclinic	Monoclinic	Triclinic	Monoclinic	Monoclinic	triclinic	triclinic
Space group	<i>P</i> 2 ₁ / <i>c</i>	<i>P</i> 2 ₁ / <i>c</i>	<i>P</i> $\bar{1}$	<i>P</i> 2/ <i>c</i>	<i>P</i> 2 ₁ / <i>n</i>	<i>P</i> $\bar{1}$	<i>P</i> $\bar{1}$
<i>a</i> / Å	11.351(2)	10.7219(19)	9.024(3)	8.764(4)	13.5527(17)	9.159(1)	8.899(2)
<i>b</i> / Å	17.803(4)	17.738(3)	11.378(3)	14.421(7)	13.4718(18)	11.115(2)	9.637(2)
<i>c</i> / Å	7.3532(16)	7.2985(13)	13.446(4)	21.802(10)	16.720(2)	11.735(2)	14.929(3)
α / °	-	-	94.809(5)	-	-	73.938(3)	84.108(3)
β / °	92.732(4)	96.290(3)	98.645(6)	92.625(8)	100.626(3)	70.770(3)	86.969(3)
γ / °	-	-	111.246(5)	-	-	69.250(3)	65.196(3)
<i>V</i> / Å ³	1484.3(6)	1379.7(4)	1257.6(6)	2752(2)	3000.4(7)	1037.5(3)	1156.1(4)
<i>Z</i>	2	2	1	2	2	1	1
<i>d</i> _{calcd} / mg m ⁻³	1.572	1.482	1.973	1.862	1.774	1.870	1.586
μ / mm ⁻¹	3.664	1.239	4.684	4.381	2.451	1.577	1.416
Reflections collected	6495	6148	5470	11815	14463	5163	5101
Independent reflections	2141 [R(int) = 0.0310]	1970 [R(int) = 0.0132]	3541 [R(int) = 0.0235]	3967 [R(int) = 0.0578]	4295 [R(int) = 0.0231]	2963 [R(int) = 0.0154]	3283 [R(int) = 0.0311]
Final <i>R</i> indices ^a	R1 = 0.0587, wR2 = 0.2014	R1 = 0.0539, wR2 = 0.1796	R1 = 0.0448, wR2 = 0.1154	R1 = 0.0519, wR2 = 0.1285	R1 = 0.0257, wR2 = 0.0821	R1 = 0.0325, wR2 = 0.0888	R1 = 0.0513, wR2 = 0.1276
[<i>I</i> > 2σ(<i>I</i>)]							

$$^a R1 = \sum ||F_o| - |F_c|| / \sum |F_o|. \quad wR2 = [\sum [w(F_o^2 - F_c^2)^2] / \sum [w(F_o^2)^2]]^{0.5}.$$

Figure captions

Figure 1. ORTEP drawing of **1**. Selected bond lengths [\AA] and angles[$^\circ$]; Mn(1)-O(1) 1.871(6), Mn(1)-O(2) 1.948(6), Mn(1)-O(2)# 1.928(6), Mn(1)-N(1) 1.959(7), Mn(1)-Cl(1) 2.694(5), Mn(1)-O(1S) 2.477(11), Mn(1)-Mn(1)# 3.013(2), Mn(1)#-O(2)-Mn(1), 102.0(2). Symmetry operation #: $-x+1, -y+1, -z+2$.

Figure 2. ORTEP drawing of **2**. Selected bond lengths [\AA] and angles[$^\circ$]; Mn(1)-O(1) 1.881(3), Mn(1)-O(2) 1.922(3), Mn(1)-O(2)# 1.948(3), Mn(1)-N(1) 1.977(4), Mn(1)-O(1)S 2.573(7), Mn(1)-Cl(1) 2.662(3), Mn(1)-Mn(1)# 3.0045(12), Mn(1)-O(2)-Mn(1)# 101.84(15). Symmetry operation #: $-x, -y+1, -z$.

Figure 3. ORTEP drawing of **3(ClO₄)₂**. Selected bond lengths [\AA] and angles[$^\circ$]; Mn(1)-O(3) 1.851(4), Mn(1)-O(2) 1.898(4), Mn(1)-O(4) 1.901(4), Mn(1)-N(2) 2.008(5), Mn(1)-O(5) 2.312(5), Mn(1)-O(1)# 2.329(4), Cu(1)-O(1) 1.896(4), Cu(1)-O(2) 1.915(4), Cu(1)-N(1) 1.948(5), Cu(1)-O(4) 2.004(4), Cu(1)-O(4)#, 2.585(4), Mn(1)-Cu(1) 2.9613(14), Mn(1)-O(2)-Cu(1), 101.91(18), Mn(1)-O(1)-Cu(1), 105.33(17), Mn(1)-O(4)-Cu(1), 98.62(17), Cu(1)-O(1)-Cu(1)#, 96.94(16), Mn(1)-O(4)-Cu(1)#, 96.17(16). Symmetry operation #: $-x+1, -y+1, -z+2$.

Figure 4. ORTEP drawing of **4(PF₆)₂·2Et₂O**. Selected bond lengths [\AA] and angles[$^\circ$]; Cu(2)-O(1) 1.898(5), Cu(2)-N(1) 1.932(6), Cu(2)-O(4) 1.952(4), Cu(2)-O(2) 1.953(5), Cu(2)-O(2)# 2.511(5), Mn/Cu(1)-N(2) 1.955(6), Mn/Cu(1)-O(2) 1.958(4), Mn/Cu(1)-O(3) 1.901(5), Mn/Cu(1)-O(4)# 1.962(4), Mn/Cu(1)-O(5) 2.319(5), Mn/Cu(1)-O(4) 2.534(5), Cu(2)-O(2)-Mn/Cu(1) 109.7(2), Mn/Cu(1)-O(4)-Mn/Cu(1)# 100.88(19), Cu(2)-O(4)-Mn/Cu(1)# 107.6(2), Cu(2)-O(4)-Mn/Cu(1) 89.93(16). Symmetry operation #: $-x, y, -z+1/2$.

Figure 5. ORTEP drawing of $5\text{Cl}_2\cdot 2\text{MeOH}$. Selected bond lengths [\AA] and angles[$^\circ$]; Mn(1)-O(7) 1.918(2), Mn(1)-O(2) 1.923(3), Mn(1)-O(5) 1.896(3), Mn(1)-O(8) 1.873(3), Mn(1)-O(7)# 2.110(2), Mn(2)-O(3) 2.271(3), Mn(2)-O(6) 2.404(3), Mn(2)-O(1)# 2.195(2), Mn(2)-O(4)# 2.124(3), Mn(2)-O(8) 2.119(3), Mn(2)-Cl(1) 2.4335(12), Cu(1)-O(1) 1.973(2), Cu(1)-O(7) 1.932(2), Cu(1)-N(1) 1.932(3), Cu(1)-O(2) 2.036(2), Cu(2)-O(4) 1.911(2), Cu(2)-O(5) 1.920(3), Cu(2)-N(2) 1.947(3), Cu(2)-O(7) 1.959(2), Cu(2)-Mn(1) 2.8550(7), Cu(1)-Mn(1) 2.8375(7), Mn(1)-Mn(1)# 2.9722(11), Cu(1)-O(1)-Mn(2)# 116.85(11), Cu(1)-O(7)-Cu(2) 127.79(12), Mn(1)-O(2)-Cu(1) 91.52(10), Mn(1)-O(7)-Mn(1)# 94.97(10), Cu(2)-O(4)-Mn(2)# 116.86(12), Cu(1)-O(7)-Mn(1)# 116.86(11), Mn(1)-O(5)-Cu(2) 96.86(11), Cu(2)-O(7)-Mn(1)# 113.14(11), Mn(1)-O(7)-Cu(1) 94.93(10), Mn(1)-O(8)-Mn(2) 118.71(12), Mn(1)-O(7)-Cu(2) 94.83(10). Symmetry operation #: $-x+2, -y+1, -z$.

Figure 6. ORTEP drawing of **6**. Selected bond lengths [\AA] and angles[$^\circ$]; Mn(1)-O(1) 1.865(2), Mn(1)-O(2) 1.873(2), Mn(1)-O(7) 1.966(2), Mn(1)-N(1) 2.021(3), Mn(1)-O(6) 2.198(2), Mn(1)-O(3)# 2.340(2), Mn(1)-Ni(1) 2.9614(7), Ni(1)-O(3) 2.006(2), Ni(1)-O(2) 2.027(2), Ni(1)-O(5) 2.032(2), Ni(1)-O(4) 2.044(2), Ni(1)-O(7) 2.0766(19), Ni(1)-O(7)# 2.094(2), Mn(1)-O(2)-Ni(1) 98.74(9), Ni(1)-O(3)-Mn(1)# 94.19(8), Mn(1)-O(7)-Ni(1) 94.16(8), Mn(1)-O(7)-Ni(1)# 103.61(8), Ni(1)-O(7)-Ni(1)# 98.19(8). Symmetry operation #: $-x+1, -y+1, -z+1$.

Figure 7. ORTEP drawing of **7**. Selected bond lengths [\AA] and angles[$^\circ$]; Mn(1)-O(3) 1.855(4), Mn(1)-O(2) 1.886(3), Mn(1)-O(1) 1.971(3), Mn(1)-N(2) 2.000(4), Mn(1)-O(4)#1 2.251(3), Mn(1)-O(9) 2.283(4), Ni(1)-O(4) 1.998(3), Ni(1)-O(2) 2.030(3), Ni(1)-O(5) 2.034(4), Ni(1)-O(1) 2.087(3), Ni(1)-O(6) 2.096(4), Ni(1)-O(1)#1 2.109(3), Ni(1)-Mn(1) 3.0758(11), Mn(1)-O(1)-Ni(1) 98.51(14), Mn(1)-O(1)-Ni(1)# 99.95(14), Ni(1)-O(1)-Ni(1)# 97.85(14), Ni(1)-O(4)-Mn(1)# 94.54(13), Mn(1)-O(2)-Ni(1) 103.45(15). Symmetry operation #: $-x, -y+2, -z+2$.

Figure 8. $\chi_m T$ vs. T plots for **1** (\square) and **2** (\circ).

Figure 9. $\chi_m T$ vs. T plots for **3**(ClO_4)₂ (\square), **4**(PF_6)₂ $\cdot 2\text{Et}_2\text{O}$ (Δ) and **5** $\text{Cl}_2\cdot 2\text{MeOH}$ (\circ).

Figure 10. $\chi_m T$ vs. T plots for **6** (\square) and **7** (\circ).

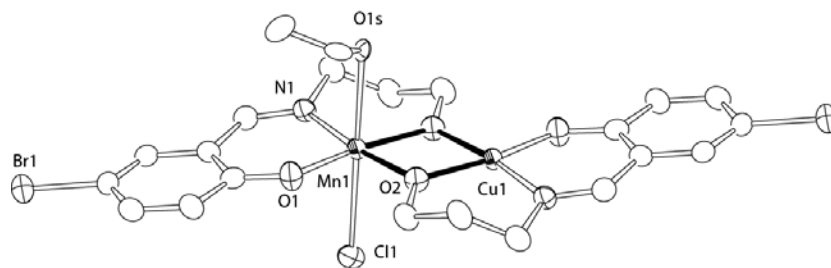


Figure 1

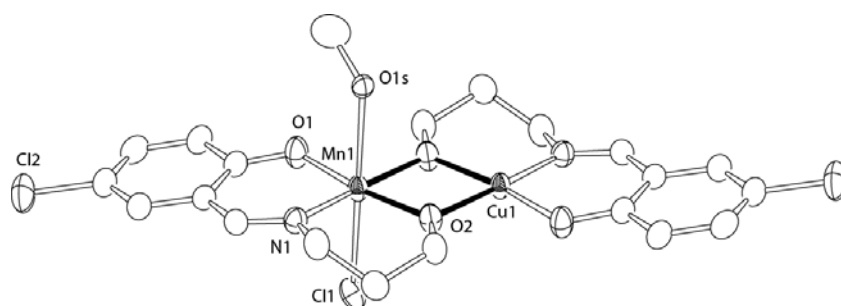


Figure 2

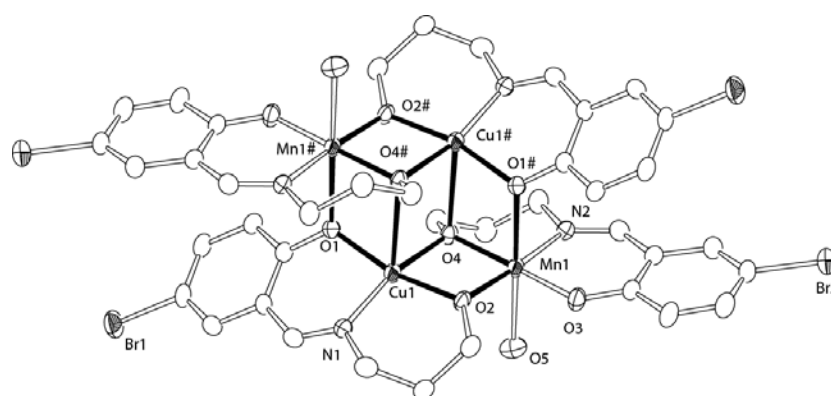


Figure 3

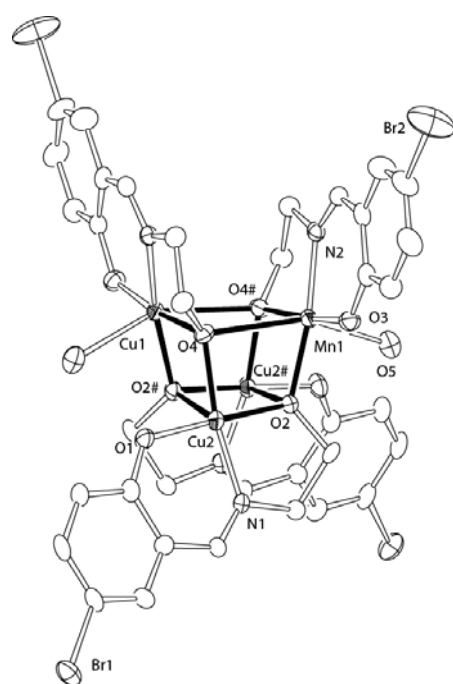


Figure 4

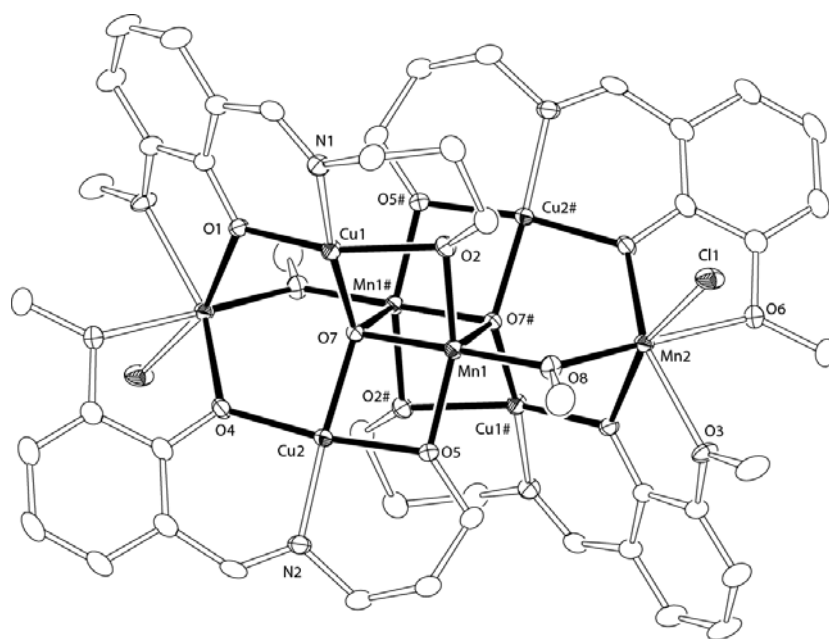


Figure 5

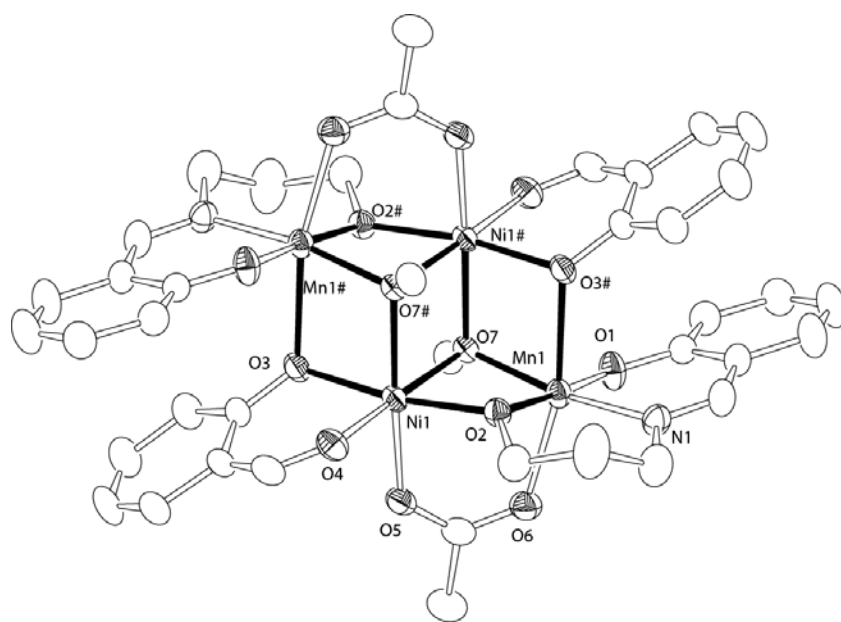


Figure 6

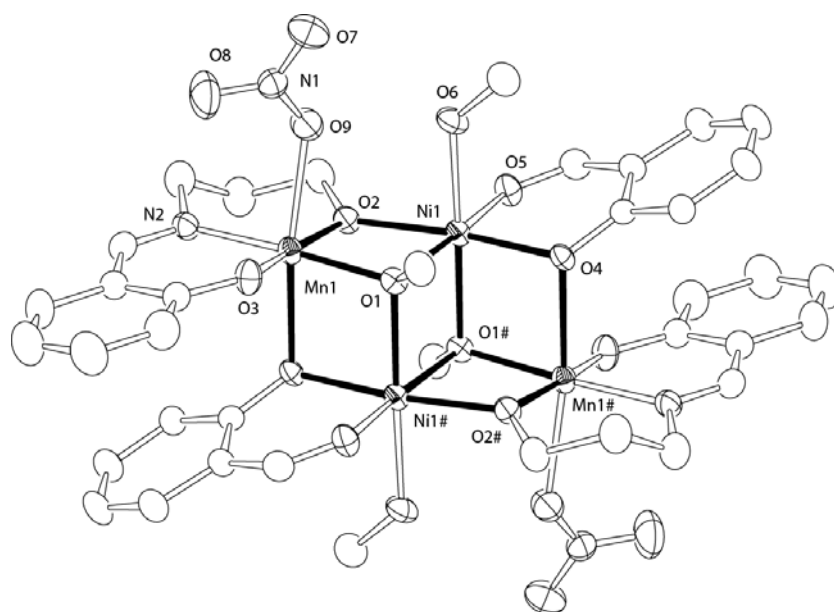


Figure 7

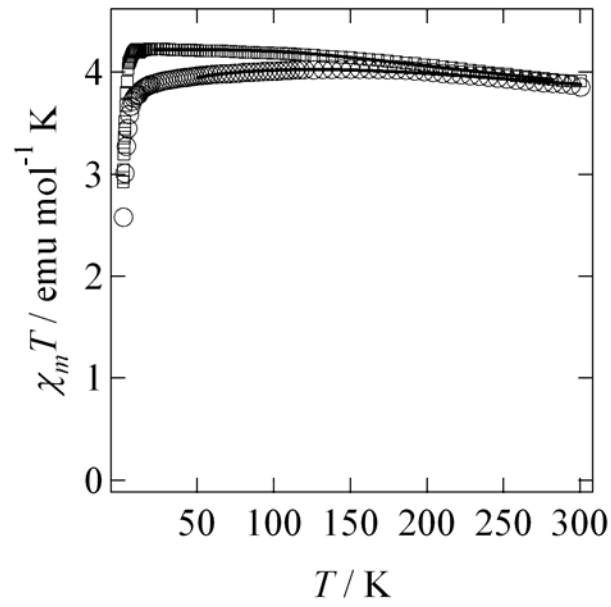


Figure 8

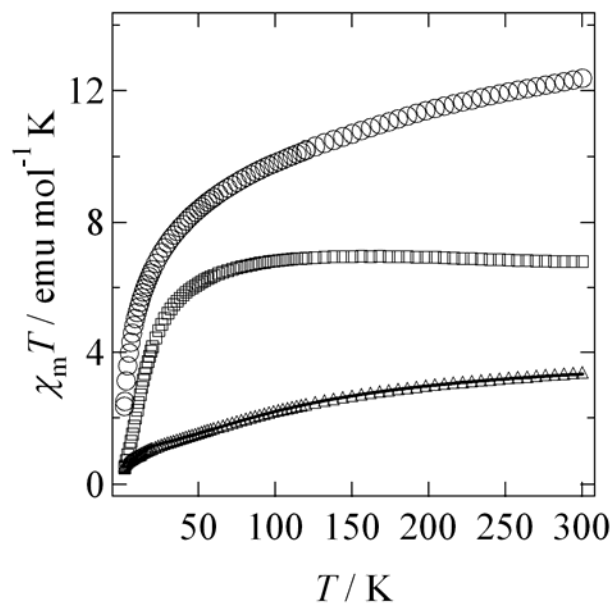


Figure 9

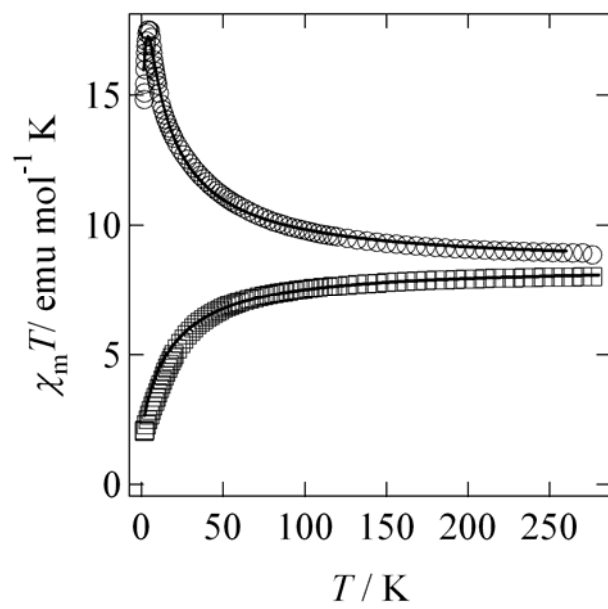
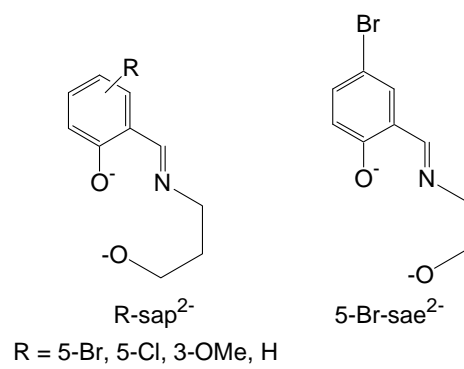
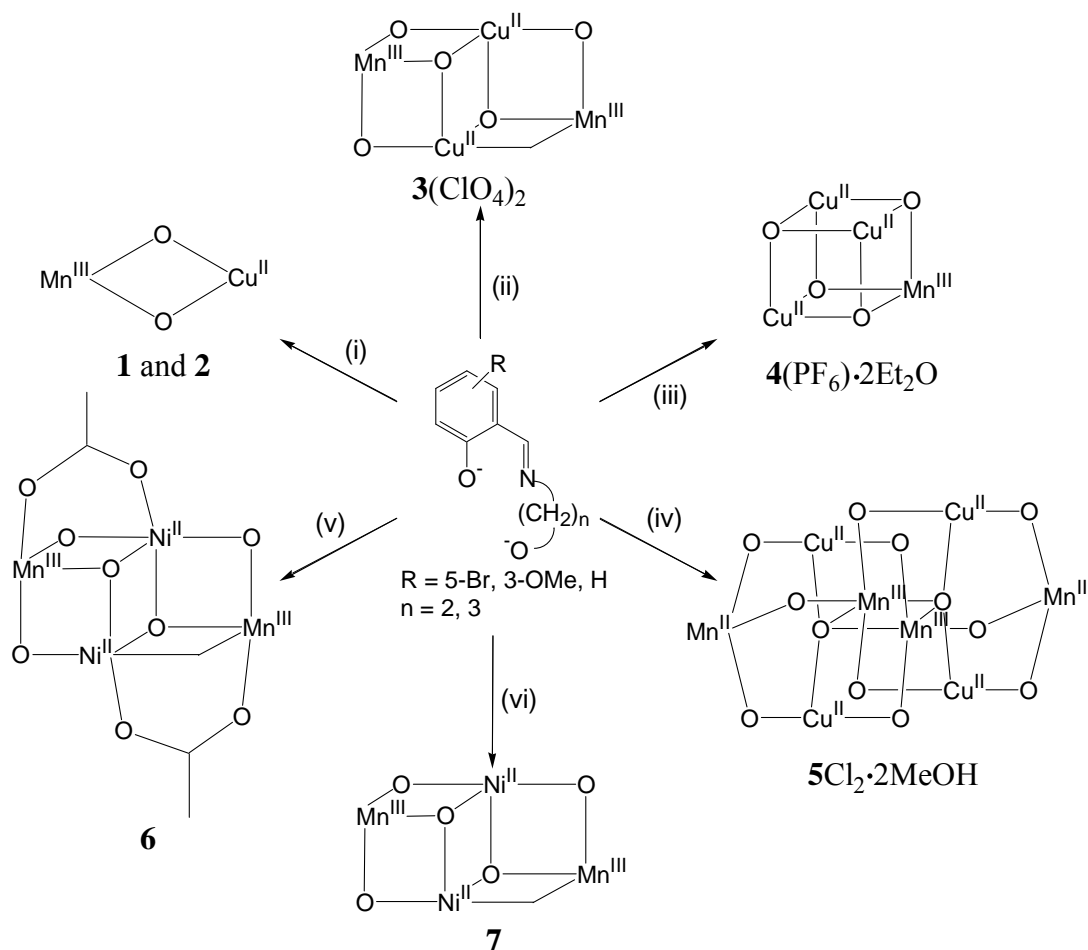


Figure 10

Scheme 1



Scheme 2



- (i) $\text{MnCl}_2 \cdot 4\text{H}_2\text{O}$, $1/3\text{CuCl}_2 \cdot 4\text{H}_2\text{O}$, MeOH, (ii) (1) $\text{MnCl}_2 \cdot 4\text{H}_2\text{O}$, $1/3\text{CuCl}_2 \cdot 4\text{H}_2\text{O}$, MeOH (2) AgPF_6 , MeCN, (iii) $\text{Mn}(\text{ClO}_4)_2 \cdot 6\text{H}_2\text{O}$, $1/3\text{Cu}(\text{ClO}_4)_2 \cdot 6\text{H}_2\text{O}$, MeCN, (iv) $\text{MnCl}_2 \cdot 4\text{H}_2\text{O}$, $2/3\text{CuCl}_2 \cdot 4\text{H}_2\text{O}$, MeOH, (v) $\text{Mn}(\text{OAc})_2 \cdot 4\text{H}_2\text{O}$, $\text{Ni}(\text{OAc})_2 \cdot 4\text{H}_2\text{O}$, sal^{1-} , MeOH, (vi) $\text{Mn}(\text{NO}_3)_2 \cdot 6\text{H}_2\text{O}$, $\text{Ni}(\text{NO}_3)_2 \cdot 6\text{H}_2\text{O}$, sal^{1-} , MeOH.

Graphical abstract

Novel Mn-Cu and Mn-Ni multinuclear hetero-metal clusters were synthesized by simple one-pot reactions of multidentate Schiff base ligands with metal sources. All clusters were selectively obtained by changing reaction conditions, suitable co-ligands, and slight modification of ligand structures. The structures and magnetic properties of these heterometal clusters were presented.

